Open access • Journal Article • DOI:10.1088/0741-3335/59/1/014046

Disruption mitigation by injection of small quantities of noble gas in ASDEX Upgrade — Source link

G. Pautasso, M. Bernert, M. Dibon, B. P. Duval ...+18 more authors

Institutions: Max Planck Society, École Polytechnique Fédérale de Lausanne, University College Cork

Published on: 01 Jan 2017 - Plasma Physics and Controlled Fusion (IOP Publishing)

Topics: ASDEX Upgrade

Disruption mitigation studies at ASDEX Upgrade in support of ITER

G. Pautasso [1], M. Bernert [1], M. Dibon [1], B. Duval [2], R. Dux [1], E. Fable [1], J.C. Fuchs [1], G.D. Conway [1], L. Giannone [1], A. Gude [1], A. Herrmann [1], M. Hoelzl [1], P.J. McCarthy [3], A. Mlynek [1], M. Maraschek [1], E. Nardon [4], G. Papp [1], S. Potzel [1], C. Rapson [1], B. Sieglin [1], W. Suttrop [1], W. Treutterer [1], the ASDEX Upgrade team [1] and the EUROfusion MST1 team [5]

[1] Max-Plank-Institute für Plasma Physik, D-85748, Garching, Germany
[2] Swiss Plasma Centre, EPFL, CH-1016 Lausanne, Switzerland
[3] Department of Physics, University College Cork, Cork, Ireland
[4] CEA, IRFM, F-13108 Saint Paul lez Durance, France
[5] http://www.euro-fusionscipub.org/mst1
E-mail contact of main author: gap@ipp.mpg.de

Abstract.

1 Introduction

The tokamak plasma can be subject to a major instability, called a disruption, which terminates the discharge [1]. Disruptions can damage machine components since they cause large mechanical forces in the conductive structures of the tokamak and large power loads onto the plasma facing components. Disruption studies address the identification of the causes leading to these instabilities, the simulation of their effects by means of physical models and the development of prediction algorithms and mitigation methods. In this way disruption studies complement fusion research activities aimed at the development and control of stable plasma scenarios.

A relatively simple but efficient method of mitigating a disruption in existing devices has been the injection of impurity material, mainly noble gas in the gaseous or frozen state, into the pre-disruptive plasma. The impurity atoms, assimilated by the plasma, radiate part of the thermal energy before it is conducted onto the divertor plates during a natural thermal quench (TQ). Moreover, the choice of the impurity type, quantity and injection scheme allows some control on the current quench (CQ) duration, indirectly on the magnitude of the mechanical forces, and on the runaway electron (RE) current generation and dissipation.

A disruption mitigation system (DMS) is also foreseen for the international experimental reactor ITER; this system is presently being designed and integrated into the overall plant system [2].

Extensive studies of disruption mitigation on the ASDEX Upgrade tokamak (AUG), using massive gas injection (MGI), have significantly contributed to the progress made in recent years in understanding the dynamics of the induced plasma shut-down (cf. [3] and references within). This understanding is a prerequisite for the formulation of appropriate mitigation schemes for ITER.

This article reports on the work of disruption mitigation - its motivation, experimental results and theoretical understanding - conducted on AUG in the last two years. The article is divided in two main sections dedicated, firstly, to the mitigation of the TQ and of the mechanical forces (sec. 2) and, secondly, to the investigation of RE generation and suppression (sec. 3). These most recent MGI experiments (sec. 2.2) have concentrated on small (relative to previous studies) quantities of noble gas injected, and particularly on the search for the minimum amount of gas necessary for a significant reduction of the vertical force, and for the mitigation of the thermal loads on the divertor before and during the TQ.

Parallel to the experimental work, the pre-thermal-quench (pre-TQ) phase, i.e. between the arrival of the gas at the plasma edge and the TQ, of different AUG MGI induced plasma termination scenarios has been simulated with the transport code ASTRA-STRAHL [4]. The code has been used to understand the experimentally observed dependence of the pre-TQ duration on the plasma and gas parameters (sec. 2.3).

Experimentally, it is found that below a given quantity of injected neon, the pre-TQ duration starts to increase abruptly and the vertical force on the machine is no longer mitigated (sec. 2.4). Moreover, the quantity of injected impurities influences the repartition between radiated and deposited power during the TQ (sec. 2.5). The toroidal asymmetry of the radiated power during the pre-TQ has been documented and shown to depend mainly on the relative position of the impurity injection location with respect to the n=1 toroidal position of the MHD modes present in the plasma before the TQ (sec. 2.6).

Studies of RE generation and suppression are rather recent in AUG. Their main result is that the injection of moderate quantities of high-Z noble gases - argon in this case - is very efficient in dissipating the RE current (sec. 3).

2 Forces and thermal quench mitigation

2.1 Background

Older (2008-2013) experiments on AUG were aimed at injecting the amount of gas necessary to reach the so-called critical density, $n_c = \mathcal{O}(10^{22})$ m^{-3}, during or just after the TQ; this value of the density would in fact assure the RE suppression in a future ITER

CQ, in spite of the expected large toroidal electric field. For this purpose, large quantities of neon atoms, i.e. $N_{inj} = 1 - 20 \times 10^{22}$, were injected into AUG plasmas (with a volume of circa 13 m^3). Nevertheless, the assimilation of gas at large N_{inj} turns out to be small [3]. In view of the difficulties encountered in present tokamaks to reach n_c, and of the limitations on the maximum allowed amount of injected gas, imposed by the capabilities of the ITER vacuum pumping and gas exhaust processing systems, the idea of mitigating TQ and suppressing RE simultaneously, with material injection before the TQ, has been abandoned [2].
The ITER DMS is now designed to consist of several material injectors, for gas and/or cryogenic pellets, which can be fired independently. A first set of injectors should provide the plasma with enough impurities to radiate most of the thermal energy during the pre-TQ and TQ, and force the current decay time to within the 50-150 ms interval; the required gas quantity is 2-3 orders of magnitude smaller than necessary to suppress REs through n_c. A second set of injectors will be devoted to suppress/control the RE beam. Crucial for the definition of the RE suppression/control scheme are relatively recent RE experiments, which show that a moderate amount of medium-high Z noble gas clearly causes or accelerates the decay of a RE beam in middle size tokamaks, such as DIII-D ([5] and references within) and AUG (this paper).

2.2 Experimental conditions and diagnostics

During the 2015-2016 experimental campaign, MGI experiments on AUG were dedicated to explore the effect of small quantities of injected neon, i.e. $N_{inj} = 10^{20} - 10^{22}$ atoms, on the evolution of the mitigated shut down. A series of target plasmas, without disruption precursors, and with different values of thermal energy, $E_{th} = 30 - 750$ kJ, were shut down by decreasing amounts of neon, in order to document any variation of the energy deposited onto the divertor and the associated change of fraction of radiated energy (sec. 2.5). Other relevant plasma parameters were: safety factor $q_{95} \sim 4.3$, plasma current $I_p = 1$ MA and magnetic energy $E_{mag} \simeq 1.4$ MJ. Reproducible disruptive scenarios with a medium-large target thermal energy (e.g. beta limit) are not available for AUG, since tearing modes typically deteriorate the thermal confinement and reduce the thermal energy before the TQ.
An additional series of ohmic plasmas ($q_{95} = 3.5$ and $I_p = 1$ MA), in which tearing modes were created by driving the plasma to the density limit and the n=1 component of the MHD modes was, on a shot-to-shot basis, locked at different toroidal angles by the RMP (resonant magnetic perturbation) coils, was terminated by circa 2×10^{21} neon atoms. The toroidal angle between the injection location and the position of the n=1 X point was scanned, in order to investigate its influence on the toroidal asymmetry of the radiated power (sec. 2.6).

The experiments were performed with one or two in-vessel valves described in [3]. The diagnostics relevant for the work presented in this article are shown in fig. 1 and will be introduced along with the discussion of the related measurements.

2.3 Pre-thermal quench phase

2.3.1 Experimental observations

The pre-TQ phase is the time interval between the arrival of the first impurity gas at the plasma edge and the start of the TQ. Its duration, Δt_{pre-TQ}, is an important parameter because it is the amount of gas, which is assimilated in this phase, that radiates part of the thermal energy before the TQ, and determines the initial current decay rate and eventually the RE generation rate. Experimentally (see fig. 2), it is found that over a wide range of neon N_{inj}, going from 10^{21} to 10^{23} atoms in AUG, Δt_{pre-TQ} decreases only by a factor of 2. Nevertheless, decreasing N_{inj} below 10^{21} neon atoms causes a rapid variation of the disruption evolution. In particular, it causes a rapid increase of Δt_{pre-TQ}, of one order of magnitude when decreasing N_{inj} from 10^{21} to 2×10^{20}. Not only the TQ occurs later, but the discharge starts suffering from minor disruptions, which can cause the loss of vertical stability of a plasma at full current.
Δt_{pre-TQ} is found to vary within a factor of two in the set of discharges with locked mode, used to study the radiation asymmetry, but to be, on average, of the same magnitude as in discharges without a locked mode. This is different (for reasons not known) from results published in [3], in which plasmas with large rotating or locked modes were found to be more unstable and exhibit a smaller Δt_{pre-TQ}.
Δt_{pre-TQ} depends very weakly on E_{th} over the whole N_{inj} range explored. This last observation does not have an intuitive explanation and has partly motivated the work of simulation of the pre-TQ phase with the 1-D ASTRA-STRAHL code, which is outlined in the following.

2.3.2 Simulation results

The 1-D transport code ASTRA, coupled with the 1-D radiation code STRAHL and the 2-D equilibrium reconstruction code SPIDER, has been used to simulate the pre-TQ phase of MGI induced shut-downs in AUG [4]. Although the fast onset of the TQ following the interaction of impurities and plasma is a 3-D process, the code ASTRA-STRAHL can reproduce the observed pre-TQ duration and its parametric dependence on several plasma and gas parameters. In addition, it shows that the cold front penetration velocity is simply determined by the total radiated power. The simulations reveal why Δt_{pre-TQ} saturates with increasing N_{inj}: injecting impurities above a given amount does

not accelerate the phase because the gas ionizes in the already cold edge region and does not contribute to the radiated power.
It is postulated that the pre-TQ ends (and the TQ occurs) when the q=2 surface is cooled down and an m=2, n=1 tearing mode grows. This physical picture is supported by diode array fast measurements of a cold and radiating front penetration. Accordingly, the pre-TQ phase is defined as the time interval necessary for the electron temperature at the q=2 surface to cool to 5 eV.
Δt_{pre-TQ} is plotted in fig. 3 versus the injected and assimilated (N_{assim}) number of neon atoms, since the code does not simulate particle loss mechanisms. In fig. 2the experimental Δt_{pre-TQ} is shown versus N_{inj}, which is a known quantity; the actual number of assimilated neon atoms is not known in this phase, since the density is toroidally and poloidally asymmetric and density measurements are available only in one sector of AUG. The assimilation fraction is estimated to be in the range 30-50 % at low values of N_{inj}; it becomes uncertain at low N_{inj} because of reasons discussed in sec. 4 of [3].

2.4 Current quench and mechanical forces

2.4.1 Current quench time

The CQ duration, Δt_{CQ}, is a parameter necessary for the design of the ITER nearby plasma-facing conductive structures, for several reasons:
• along with the plasma vertical movement, Δt_{CQ} determines the magnitude of the induced eddy currents and related mechanical stresses in the first-wall and blanket modules;
• in competition with the growth rate of the plasma vertical displacement, it determines the vertical force on the vessel and other stabilizing components, through halo and induced toroidal currents;
• Δt_{CQ} determines the toroidal electric field, which tends to generate the runaway electrons.
Δt_{CQ} is mainly determined by the energy balance $P_{rad} \simeq -dE_{mag}/dt$ (with P_{rad} being the radiated power). In particular, the area-normalized current decay time, i.e. $\Delta t_{CQ}/S$ (where S is the area of the plasma poloidal cross section), is a proxi for the plasma resistivity during the CQ and has been used for cross-machine comparison of Δt_{CQ} and extrapolation to ITER. The CQ time in ITER will have to be tailored in the range Δt_{CQ} = 50 - 150 ms, or equivalently $\Delta t_{CQ}/S$ = 2.3 - 7.0 ms/m^2 (with S = 21.3 m^2 being the area of the ITER plasma poloidal cross section) in order to avoid large eddy currents and large vertical forces.
The definition $\Delta t_{CQ} \equiv (t_{20} - t_{80})/0.6$ is used here, with t_{80} and t_{20} being the times at which the I_p has decayed to 80 % and 20 % of its pre-disruption value respectively.
The minimum value of $\Delta t_{CQ}/S$ in AUG is about 2 ms/m^2 and is reached in natural

disruptions during vertical displacement events (VDEs). As shown in fig. 4, the present series of mitigated disruptions has an area-normalized current decay time decreasing with increasing N_{inj} and is within the "prescribed ITER range". This result suggests that mitigation of the eddy currents and of the vertical force should be possible in ITER over a wide range of N_{inj}. Only at $N_{inj} < 4 \times 10^{20}$ does the experimental data approach the upper end of the prescribed Δt_{CQ} ITER range. The scatter of the data-points at these lower values of injected gas (fig. 4) is due to the appearance of minor disruptions, which can induce a VDE and a short CQ, caused by the cooling effect of the strong interaction divertor-plasma and not by MGI.

2.4.2 Halo current and vertical force on the vessel

The total vertical force on the AUG vessel is the sum of the forces generated by the halo currents, flowing mostly poloidally in the vessel between the inner and outer divertor plates, by the toroidal current induced in the passive stabilizing loop (PSL) and by the toroidal current flowing in the vessel.
AUG is equipped with shunts for the measurement of halo currents (I_{halo}) in the lower divertor. Halo currents of up to 40 % of the pre-disruption plasma current have been observed in unmitigated disruptions. Impurity injection reduces the maximum halo current because it accelerates the toroidal current decay after the TQ and prevents the formation of a halo region carrying a large toroidal (and therefore poloidal, since the current flows parallel to the magnetic lines) current. The reduction of I_{halo} following the increase of N_{inj} is shown in fig. 5. Its monotonic but steplike behavior can be understood from fig. 6. This figure shows the value of the current of the plasma at the time it has moved vertically (towards the lower divertor in these cases) by 25 cm from the pre-disruption position. These plasmas had an initial current of 1 MA. For $N_{inj} \leq 10^{21}$,approximately 40 % of I_p has decayed while the plasma has moved of 25 cm. For $N_{inj} > 3 \times 10^{22}$ the CQ occurs while the plasma is still centred in the machine, because the CQ becomes faster than the vertical displacement.
AUG is also equipped with strain gauges on the vessel suspension roads: they record a total vertical force, F_{vv}, in the range $-100 \div 100$ kN for $N_{inj} > 10^{21}$, increasing in absolute value as the neon amount is reduced. The vacuum vessel oscillates after the disruption and fig. 7 shows the maximum and the minimum F_{vv} values reached as N_{inj} varies. In past unmitigated disruptions, $|F_{vv}/I_p|$ has reached 600 kN/MA. The vertical force acting on the PSL is presently not measured and therefore not discussed here.
A reduction of the mechanical forces following MGI in AUG cannot be extrapolated to ITER without self consistent modeling of the whole plasma-conductor interaction. Therefore the benchmark and model development of appropriate numerical codes (e.g. TSC and DINA) is an on-going activity within the ITPA MHD topical group.

2.5 Thermal loads

One of the purposes of the work presented here is to document the influence of N_{inj} on the repartition of the plasma energy dissipated during a disruption: In fact, it is to be feared that a reduction of the injected impurity amount could result in a reduction of the fraction of the radiated power and into an increment of the fraction conducted onto the divertor plates.

AUG is equipped with several foil-bolometers, located in one toroidal sector (fig. 1), measuring the radiated power with a time resolution of one ms. Diode-bolometers, located in two toroidal sectors 180^o apart, allow for finer time resolved measurements of photon emission during the pre-TQ and the TQ; nevertheless they must be calibrated by comparison with the foil bolometer.

The power deposited on a small area (15 x y cm^2) of the outer divertor (P_{div}), about the strike point of the target plasma separatrix has been measured every 0.4 ms (following a trade-off between time resolution and area) by an infra-red camera. The foot-print of the heat flux onto the divertor is localized within the viewed area during the pre-TQ. However, during the TQ, the heat flux onto the divertor is deposited on a poloidally broader surface; nevertheless localized measurements can still be significant.

The energy radiated (E_{rad}) during the whole pre-TQ and TQ phase is plotted on the left of fig. 8 versus the energy available for dissipation during this phase. E_{rad} is measured by the diode-bolometers and averaged over the two toroidal sectors. The available energy is defined to be $(E_{th} + 0.05 \times E_{mag} + E_{in})$, with E_{in} being the total auxiliary power. This figure indicates that the amount of energy available for dissipation is mostly radiated and found as E_{rad}, independent of E_{th} or N_{inj}: therefore a decrease in N_{inj} does not clearly result into a decrease of E_{rad}.

E_{rad}/E_{th} does decrease with N_{inj}, independently of E_{th}, during the TQ (fig. 8, right). Nevertheless, this tendency is due, in several discharges, to a larger fraction of E_{th} being radiated during the pre-TQ (fig. 8, centre), because the plasma is more stable or undergoes several minor disruptions, and to a smaller E_{th} available at the beginning of the TQ. In this case, the TQ is defined as the 1 ms time interval about the maximum value of P_{rad}.

The data points at $N_{inj} \sim 2 \times 10^{21}$, rising above the others on the right of fig. 8, pertain to target plasmas with a very low E_{th} (< 0.1 MJ). E_{rad}/E_{th} is larger than unity in these cases probably because a fraction of E_{mag} is also being radiated. The same explanation applies to this set of data points in fig. 9.

No clear trend of E_{rad}/E_{th} is seen during the pre-TQ phase (fig. 8, centre).

The hypothesis that the ratio of conducted to radiated energy increases in the pre-TQ and in the TQ, when less gas is injected, is not confirmed for all cases by the bolometric measurements. However, the thermography measurements indicate that a larger fraction

of thermal energy can be deposited in the divertor during the TQ. Fig. 9 shows two branches of E_{div}/E_{th} at low N_{inj}: the upper data points pertain to TQs, which consist of one single (radiated and deposited) energy spike, while the plasmas of the lower set lose energy with a sequence of bursts. E_{div} in this figure is defined as the energy measured on the mentioned divertor area during 1 ms about the maximum P_{div}.
In AUG, thermography measurements suggest that $N_{inj} > 10^{21}$, with $N_{assim} \simeq 0.3 \div 0.4 \times N_{inj}$, are required to insure thermal load mitigation on the divertor plates. ASTRA-ZIMPUR simulations, presented in [6], indicate that $N_{assim} > 2 \times 10^{22}$ of neon are necessary to mitigate an ITER TQ. JET results presented in [7] show a decrease of the fraction of the radiated power over the whole disruption at $N < 4 \times 10^{21}$ of neon injected before the TQ (and assimilated?) in a mixture of 90 % D_2 and 10 % Ne. These numbers suggest that, the neon amounts necessary for heat load mitigation in AUG, JET and ITER scale roughly with the plasma volumes, i.e. $V_{AUG} : V_{JET} : V_{ITER} = 13 : 100 : 840$ m^3.
At this point we can conclude that the minimum quantity of assimilated gas, necessary for the mitigation of the thermal load and of the mechanical forces in ITER, and how it will depend on the use of either pellets or gas, must still be confirmed by further experiments and extrapolation through modelling.

2.6 Asymmetric radiation distribution during the pre-TQ

During the pre-TQ, both the injected impurities and the radiated power density, $\mathcal{P}_{rad}$, are strongly poloidally and toroidally asymmetric, and typically larger in the vicinity of the valve. The presence of rotating MHD modes - and probably also the plasma rotation, carrying the impurities toroidally away from the injection location - can reduce the toroidal asymmetry of the energy radiated in this phase. During the TQ, both density and radiation asymmetries decrease, suggesting that a mixing of the impurities in the plasma takes place.
The spatial distribution of the radiated energy is studied in existing tokamaks, motivated by the report in [8] that an increase of a factor of two in the energy deposited on the wall with respect to the energy assumed uniformly radiated during an ITER pre-TQ ($E_{th} = 350$ kJ within 1 ms) would melt the Be wall.
A key reference for the interpretation of the radiation asymmetry after MGI is [9]: simulations performed with NIMROD pointed out that the relative position of valve, with respect to the n=1 X point, strongly influences the magnitude of the asymmetry; in particular, the maximum $\mathcal{P}_{rad}$ occurs when the impurities are injected into the X point of the n=1 existing modes.
Ohmic plasmas, with tearing modes induced by density limit, were used to document the variation of radiation asymmetry (see also sec. 2.2). The modes, with a typically

dominant n=1 toroidal number, were intentionally locked by a resonant n=1 magnetic field created by the RMP coils at different toroidal positions. Neon injection into the plasmas was triggered by the locked mode trigger, once the amplitude of n=1 component of the radial magnetic field ($\tilde{B}_{r,n=1}$) exceeded a given threshold.
The magnitude of the ratio of the energies radiated in two toroidally opposite sectors (the valve is positioned at $\Phi = 0$), $E_{rad}(\Phi = 0)/E_{rad}(\Phi = \pi)$, reaches the values of 4 and 2.5 during the pre-TQ and during the TQ respectively. This ratio exhibits a sinusoidal curve, as shown in fig. 10 versus the position of the maximum $\tilde{B}_{r,n=1}$, as measured by the saddle coils on the HFS.
The effect of rotation on the asymmetry is suppressed and the effect of toroidal spreading of the impurities - due to parallel thermal velocity - is limited by the low plasma temperature in this dedicated experiment. This data-set is particularly suited for the benchmark of 3-D non-linear MHD codes, such as JOREK, which is being further developed for disruption modelling [10]. In previous experiments [11], it was found that plasmas at larger energies could not be stopped by the RMPs and therefore the radiation asymmetry was affected by a residual, difficult to measure, rotation.

3 Generation and dissipation of REs

3.1 Background

Runaway electrons (REs) are expected to be generated in ITER disruptions at full plasma current [2]. While the generation mechanisms of REs are relatively well understood, there is no general consensus on which loss mechanisms are dominant in present experiments, and which will prevail in ITER. This makes the calculation of the expected RE current and energy - and the consequent damage to the plasma facing components - uncertain and the design of the ITER disruption mitigation system challenging.
AUG disruptions, typically of diverted and elongated plasmas, do not exhibit the formation of RE beams, consistent with theoretical expectations. Therefore, in order to allow studies of RE generation and dissipation during disruptions, a scenario for RE generation during the TQ had to be - and was - established during the 2014 campaign [12], and further extended and explored in 2015. The main aim of the 2015 experiments was to explore the possibility of influencing the RE generation and losses within the range of variability of machine and plasma parameters. This paper concentrates on one aspect of the available analysis, namely on the RE current suppression by argon MGI and the evaluation of the friction force on the REs.

3.2 Experimental scenario and measurements

[Update all the numbers - still 2014]

REs have been generated by injecting between 0.07 and 0.2 bar×litre of argon in a low target density (volume averaged $n_e < 2\times10^{19}$ m^{-3}) circular limiter plasma, with a current of 0.8 MA, a toroidal magnetic field of 2.5 T and 2 MW of ECRH heating. The injected argon induces a fast quench of the current carried by thermal electrons, followed by a long-lived runaway beam, forming a toroidal current of up to 300 kA, and lasting up to 380 ms. The RE beam current and duration are found to be reproducible. Nevertheless, changes in the current ramp up history influence the RE current/duration, supposedly because of changes in the current profile and the resulting MHD activity before and during the TQ.

Changes in the toroidal magnetic field and therefore in the safety factor, in the deposited ECRH power and deposition location, in the heating and current drive scheme, in the reference current imposed by the control system, and the application of RMPs were also undertaken. These studies must be further exploited and extended; therefore, the related experimental results will not be discussed in this article.

The circular plasma carrying the RE beam is vertically stable. The plasma position and the shape, deduced from equilibrium reconstruction, are in agreement with Soft X-Ray profiles. The plasma control system does not contribute to the beam vertical stability because the current in the control coils is for part or all of the time saturated. A slow vertical displacement of the RE beam sets-in only in a few cases and does not affect the overall RE current decay rate.

The plasma-RE current is controlled by the control system. After injection of "small" amounts of argon, the controlled current follows the pre-programmed waveform; larger amounts of argon increase the RE losses, accelerate the current decay with the result that the OH system cannot keep the actual current at the level of the reference value.

Line integrated measurements of the electron density, n_e, are available during the whole RE beam lifetime from 5 DCN interferometer chords and from 2 CO2 chords. The n_e profiles could be reconstructed for all the discharges during most of the RE beam because a magnetic equilibrium is available.

The foil bolometers measure a total radiated energy of the order of magnitude of the initial kinetic and magnetic energy of the RE beam. This suggests that radiation plays a significant role in the RE energy dissipation. Measurements of Bremsstrahlung are not available for this dedicated experiment. Synchrotron radiation spectra were recorded with a system developed at ENEA-Frascati and similar to the one used on FTU [13].

Time-resolved measurements of gamma spectra from a gamma/neutron spectrometer are available and can give indication of the RE energy spectra, if interpreted with a model of RE-matter interaction. The gamma spectrum is peaked at energies of circa 100 keV

and does not change its form significantly as the RE current decays. The reconstruction of the energy distribution function from these measurements is in progress.

3.3 RE suppression

3.3.1 Experimental results

In some of the RE beams generated, argon was injected a second time (0.17 and 0.7 bar×litre with a second valve) with a delay of 70 ms from the first argon puff. Both an in-vessel valve, with the nozzle some 10 cm far away from the plasma edge, and an electromagnetic valve, 1.5 m far away, were used. The RE current life time, Δt_{RE}, after both the first and the second argon puff, show a clear dependence on the argon amount injected - i.e. the more gas the faster the decay - as illustrated in fig. 11. The RE current does not exhibit a regular monotonic decay but rather a "bumpy" time behavior; therefore Δt_{RE} is here simply defined as $\Delta t = 2 \times (I_{RE,0} - I_{RE,end})/((I_{RE,end} + I_{RE,0})$. The final phase of the current is often characterized by a faster loss of 30-100 kA, followed again by the slower decay of the residual current, < 30 kA. Δt_{RE} is evaluated by taking $I_{RE,end} = 30$ kA for all discharges. $I_{RE,0}$ is the RE current after the 1st or 2nd argon injection.
Fig. 11 suggests that RE collisions with the electrons and the high Z impurity atoms is a significant RE current dissipation mechanism. In the following section, the from current decay observed and from density measurements inferred collisional damping are discussed.

3.3.2 RE collisional damping

REs lose energy through different known mechanisms: By inelastic collisions mainly with bound and free electrons, through small angle scattering and transfer of energy to the matter in which they travel; by collisions with ions and Bremsstrahlung radiation; and by cyclotron and synchrotron radiation. The first mechanism, i.e. the friction force of the electrons on the REs, is discussed in this contribution, since the loss of energy by the other mechanisms has not been evaluated yet (although they are believed to be smaller). The correct modelling of the evolution of the RE population requires kinetic calculations. Nevertheless, at least formally, the RE current time evolution (with time constant τ_{RE}) is expected to be described by

$$\frac{1}{\tau_{RE}} = \frac{dI_{RE}}{dt}\frac{1}{I_{RE}} = \frac{dn_{RE}}{dt}\frac{1}{n_{RE}} \simeq \frac{e(E_\phi - E_c)}{p_{RE}} \tag{1}$$

where E_ϕ is the toroidal electric field, E_c is the so-called critical electric field, n_{RE} is the RE density and p_{RE} is the average RE momentum. Therefore the magnitude of E_ϕ and E_c are discussed in the following.

Toroidal electric field. The evaluation of E_ϕ in the plasma requires a self consistent modelling of the plasma current evolution, which is mainly carried by the REs in the analysed discharges. Numerical modelling has not been carried out yet and therefore the time evolution of the E_ϕ profile in the plasma in not known. Nevertheless, measurements of the loop voltage (U_{loop}) at different poloidal positions around the plasma are available. The closest - to the plasma - U_{loop} coil is inside the vessel, behind the inboard heat shield, some 10 cm distant from the the plasma surface.
An average E_ϕ can also be calculated knowing the plasma self-inductance and the multual-inductance between the plasma and other coils/structures:

$$2\pi R_c E_\phi \simeq L_p \frac{dI_p}{dt} + M_{OH-p}\frac{dI_{OH}}{dt} + M_{vv-p}\frac{dI_{vv}}{dt} \tag{2}$$

where M_{OH-p} and M_{vv-p} are the mutual inductances between the OH coils and the plasma, and between the vessel structures and the plasma, respectively. The U_{loop} measurements and the estimations with Eq. (2) give the following consistent picture: during the CQ, transient U_{loop} values of 40-50 V are reached; during the RE plateau, the loop voltage decreases from 10 to a few V in all cases; during the fast RE termination caused by the second argon injection, transient U_{loop} up to 10 V are generated. $E_\phi = U_{loop}/(2\pi R_c) \sim U_{loop}/10$, with a current major radius, $R_c \sim 1.6$ m.
Critical electric field. E_c is a linear function of the free and bound electron density; therefore its estimation requires knowledge of the plasma atomic species and their ionization state:

$$E_c = e^3 n_e ln(\Lambda_{e,free})/(4\pi\epsilon^2 m_e c^2), \qquad n_e = n_{e,free} + \frac{ln(\Lambda_{e,bound})}{ln(\Lambda_{e,free})} n_{e,bound} \tag{3}$$

Impurities other than argon are neglected here.
Argon concentration. Several spectrometers were configured to record line emission from Ar-I, Ar-II, C-II and C-III during the RE beam. The line integrated measurements of light emitted by specific transitions allow a spatially resolved calculation of the argon and carbon densities and of the electron temperature (T_e) once the free electron density is known, since the line radiance, L, is given by the following integral along the line of sight:

$$L = \frac{1}{4\pi}\int n_e\, n_z\, f_z\, X_{eff}\, dl \tag{4}$$

The photon emissivity coefficients, X_{eff}, for the relevant transitions have been calculated from a collisional radiative model. The model considers only the population of the upper states by electron excitation collisions; for the solution of the collisional radiative model, the ADAS208-code [14] has been used. The fractional abundances of carbon and argon, f_z, have been calculated from the ADAS data sets for rate coefficients of ionization and recombination, assuming a balance of ionization and recombination rates. An additional

data set, derived from data available at [15], were also computed and show a somewhat different ratio f_{Ar-I}/f_{Ar-II}.
The comparison between the line integrated emission of C-II and C-III and the respective $(f_z\, X_{eff})$ factors suggests $T_e \leq 1.8$ eV. At this temperature the argon and carbon are expected to be mostly singly ionized. Indeed, the measurements of C-III are at or below the noise level, indicating no significant concentration of this carbon ionization state; Ar-I is also clearly present over the whole plasma. Together both observations suggest a $T_e < 2$ eV. The comparison between the line integrated emission of Ar-I and Ar-II and the calculated $(f_z\, X_{eff})$ factors is not conclusive, since the two sets of f_z suggest rather different T_e values.
With the uncertainties just discussed, an argon concentration of around 100 % is derived from Eq. 4 using the measurements of Ar-II radiation for the specific discharges analyzed. This order of magnitude is consistent with the ratio of 10:1 between the quantities of argon and deuterium injected in one discharge.
Critical versus toroidal electric field. Fig. 12 summarizes the comparison between the measured E_ϕ and E_c induced from the argon density estimates and n_e measurements (at different times after the CQ). The critical electric field is typically larger than the toroidal electric field sustaining the RE beam, and therefore significantly accounts for the RE energy losses associated with the observed current decay.
Although large error bars affect the estimated argon concentration and thus of E_c - because of uncertain radiation coefficients - we can conclude that the plasma composition of the AUG RE beams is different from the one obtained at DIII-D. The RE beams have a smaller argon concentration [5] and anomalous RE current dissipation mechanisms, one order of magnitude more efficient than e-RE collisions, have to be invoked to explain the observed RE current decay rate. The AUG result does not exclude a significant role of the RE-ion collisions in the decay of the RE current or the presence of other loss mechanisms; nevertheless these mechanisms would have an effect quantitatively comparable to the effect of the e-RE collisions.

4 Summary

The range of neon quantities injected in AUG plasmas during MGI experiments has been extended below the minimum quantity necessary for disruption mitigation and the influence of these quantities on the induced plasma-shutdown have been analyzed and documented.
1-D modelling of the pre-TQ phase, performed with the code ASTRA-STRAHL, reproduces its duration and the parametric dependences observed experimentally. The code can therefore be used to determine ITER pre-TQ. The cooling of the q=2 surface below

5 eV is a good criteria for the TQ onset.
The observed CQ duration is in the prescribed ITER range over a wide range of N_{inj} values. Forces and heat load are mitigated in AUG with $N_{inj} > 10^{21}$ atoms of neon. At lower quantities of gas the forces increase towards the unmitigated values.
Thermography data provide experimental indication that more energy is deposited during the TQ as the gas amount is decreased. A more extensive monitoring of the surfaces exposed to the plasma and 3-D non-linear MHD calculations are necessary to predict power loads in an ITER disruption. The problem of characterizing the thermal loads during disruptions has been and remains complex. The 3-D nature of the energy flow and dissipation, the large surface area affected by energy deposition, the limited surface area monitored by the diagnostics and the errors affecting the measurements are some of the reasons why the treatment of this problem is never conclusive.
A scenario for the generation of runaway electrons during the CQ has been established by injecting small quantities of argon into a low density target plasma and it allows for the study of runaway formation and losses. The main finding is that the quantity of argon injected, to create and then suppress the REs, has a clear influence on the time decay of the RE beam, i.e. the more impurities, the faster the RE current decay. The critical electric field, calculated from the electron density and the concentration of argon, is larger than the toroidal electric field sustaining the RE beam, and thus significantly accounts for the RE energy losses associated with the observed current decay. Large error bars affect the estimated argon concentration because of uncertainties in the radiation coefficients.

Acknowledgements.
The first author acknowledges useful discussion with Michael Lehnen (IO). This project has received funding from the European Unions Horizon 2020 research and innovation programme under grant agreement number 633053. The views and opinions expressed herein do not necessarily reflect those of the European Commission.

References

[1] T.C. Hender et al., Nuclear Fusion, 47 (2007) 128-202

[2] M. Lehnen et al., Journal of Nuclear Material, 463 (2015) 39

[3] G. Pautasso et al., Nuclear Fusion, 55 (2015) 033015

[4] E. Fable et al., Nuclear Fusion, 56 (2016) 026012

[5] E.M. Hollmann et al., Physics of Plasma, 22, 021802(2015)

[6] V. Leonov et al., contribution P2.108, in 38^{th} EPS Conference on Plasma Physics (2011) Strasbourg, France

[7] S. Jachmich, *Disruption mitigation at JET using massive gas injection,* in 43^{ed} EPS Conference on Plasma Physics (2016) Leuven, Belgium

[8] M. Sugihara et al., Nuclear Fusion, 47, 337 (2007)

[9] V. Izzo et al., Physics of Plasmas, 20, 056107 (2013)

[10] E. Nardon, et al., *Progress in understanding disruptions triggered by massive gas injection via 3-D non-linear MHD modelling with JOREK,* in 43^{ed} EPS Conference on Plasma Physics (2016) Leuven, Belgium, submitted to PPCF

[11] G. Pautasso et al., *MGI in plasmas with locked modes,* Proc. 40th European Physical Society Conference on Plasma Physics (Espoo, Finland, 2013), paper O5.104

[12] G. Pautasso et al., *Generation and suppression of runaway electrons in ASDEX Upgrade disruptions,* 42nd EPS Conference on Plasma Physics, 22-26 June 2015, Lisbon, Portugal

[13] B. Esposito et al., *Runaway electron generation and control,* in 43^{ed} EPS Conference on Plasma Physics (2016) Leuven, Belgium, submitted to PPCF

[14] H.P. Summers, ADAS User Manual 2.6 (2004). http://www.adas.ac.uk./manual.php

[15] FLYCHK: Generalized population kinetics and spectral model for rapid spectroscopic analysis for all elements, H.-K. Chung, M.H. Chen, W.L. Morgan, Y. Ralchenko and R.W. Lee, High Energy Density Physics, Volume 1, Issue 1, December 2005, Pages 3-1

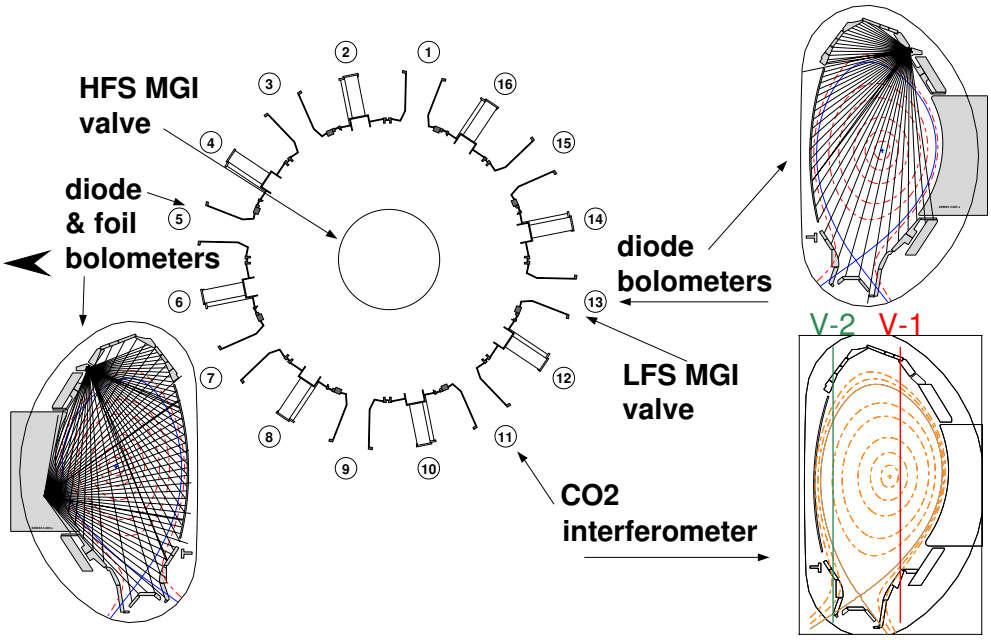

Figure 1: Overview of AUG diagnostics relevant for disruption studies.

[Add thermography, spectrometers, RMP coils, LM coils]

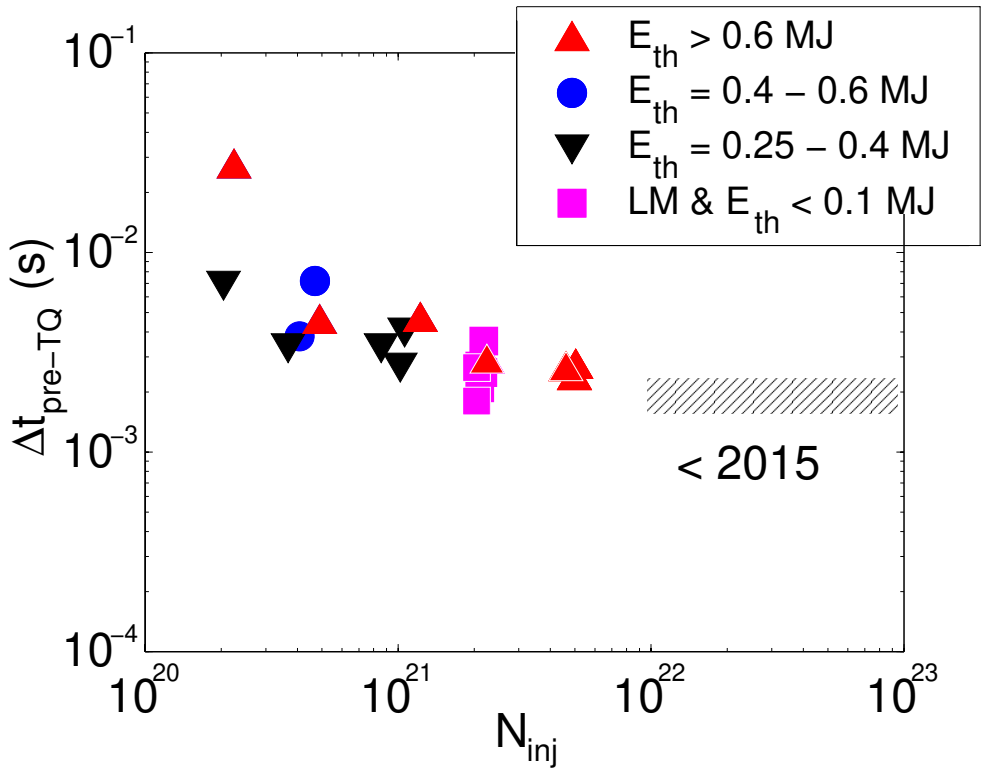

Figure 2: Pre-TQ duration (Δt_{pre-TQ}) versus the injected number of neon atoms injected (N_{inj}) for different ranges of plasma thermal energy (E_{th}). The hatched area represents older results published in [3].

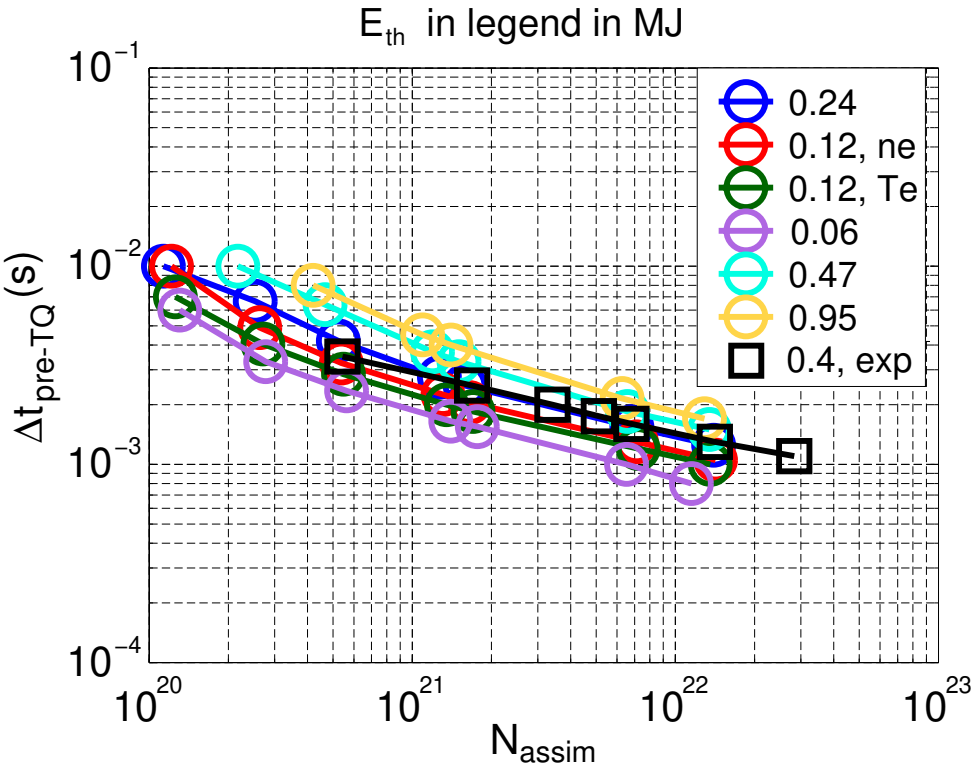

Figure 3: Duration of the pre-TQ phase (Δt_{pre-TQ}), simulated by ASTRA-STRAHL, versus the assimilated number of neon atoms (N_{assim}) for different values of the plasma thermal energy (E_{th}).

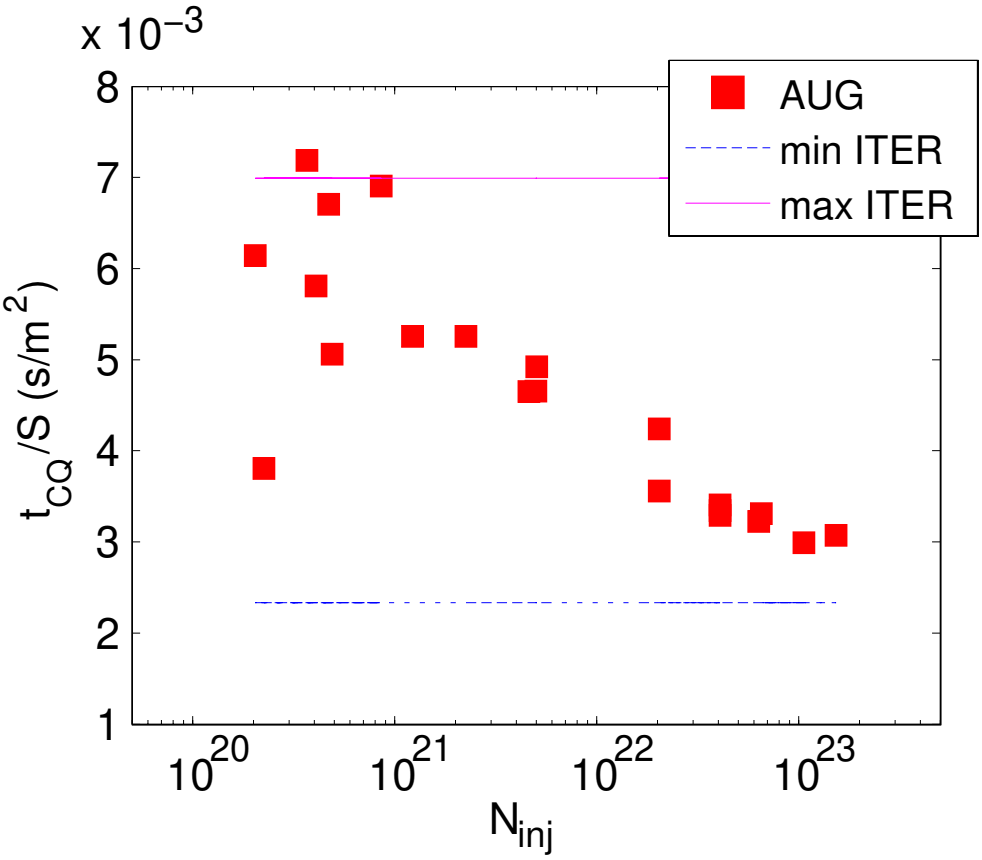

Figure 4: Area-normalized current decay time (t_{CQ}/S) versus the number of injected neon atoms (N_{inj}). The horizontal lines represent the upper and lower boundary of the t_{CQ}/S interval prescribed for ITER.

[Show also figure w time traces]

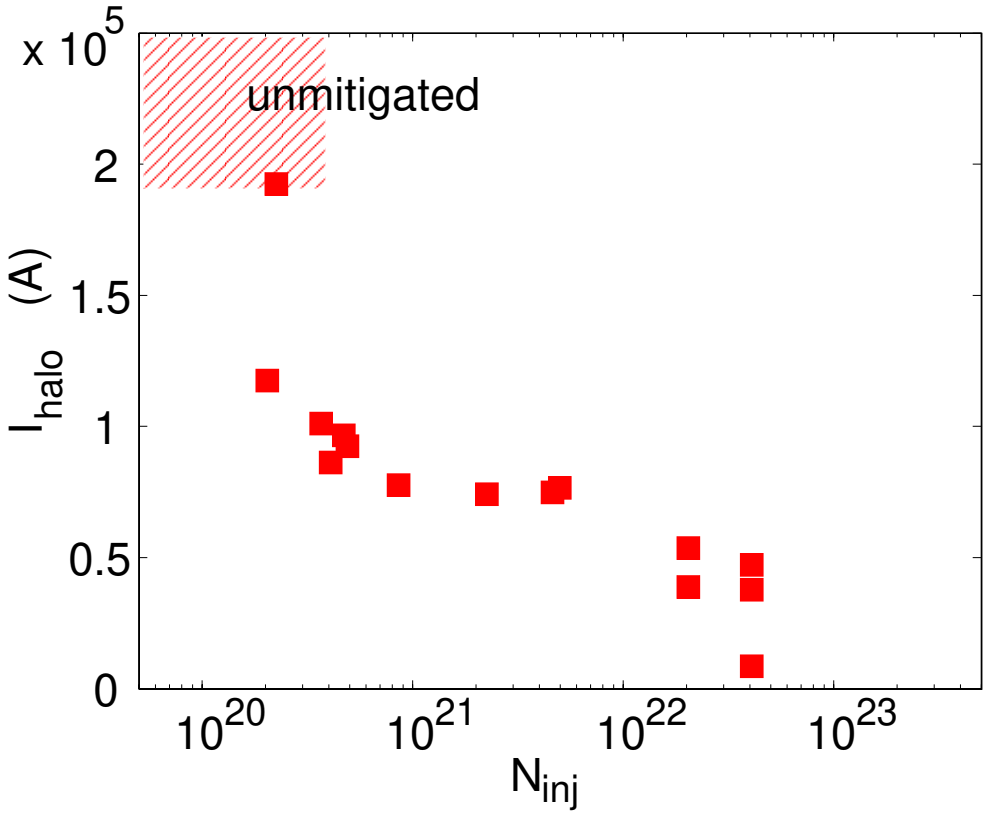

Figure 5: Halo current (I_{halo}) versus the number of injected neon atoms (N_{inj}).

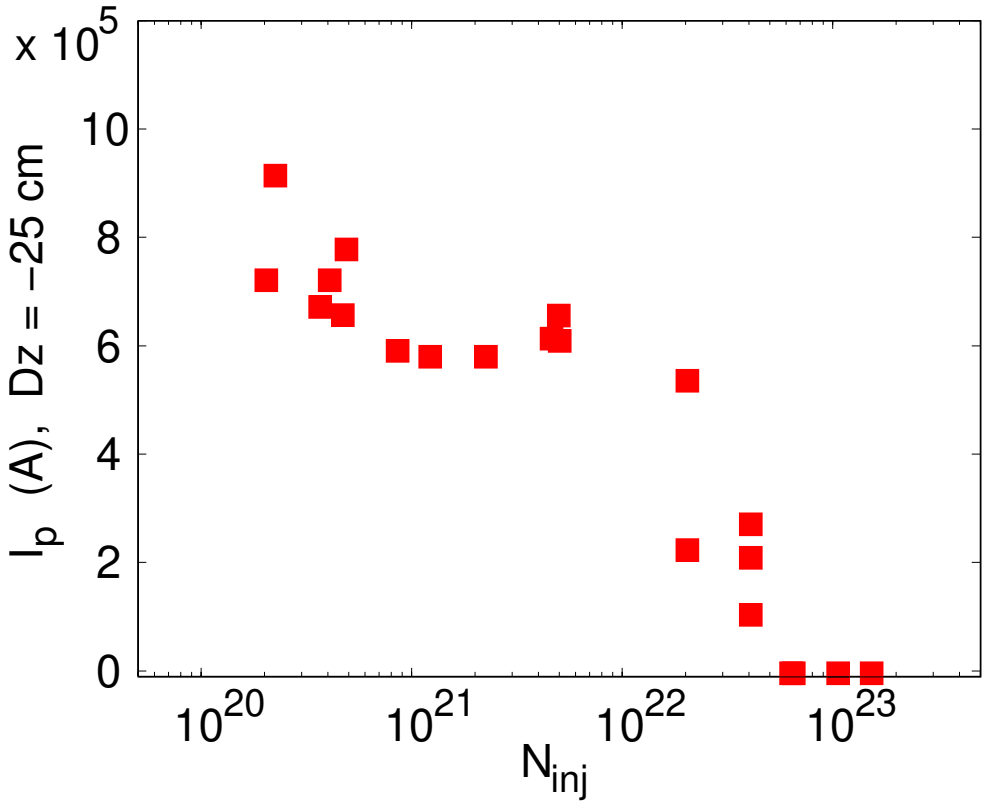

Figure 6: Toroidal current (I_p), carried by the plasma which underwent a vertical displacement (Dz) of 25 cm, versus the number of injected neon atoms (N_{inj}).

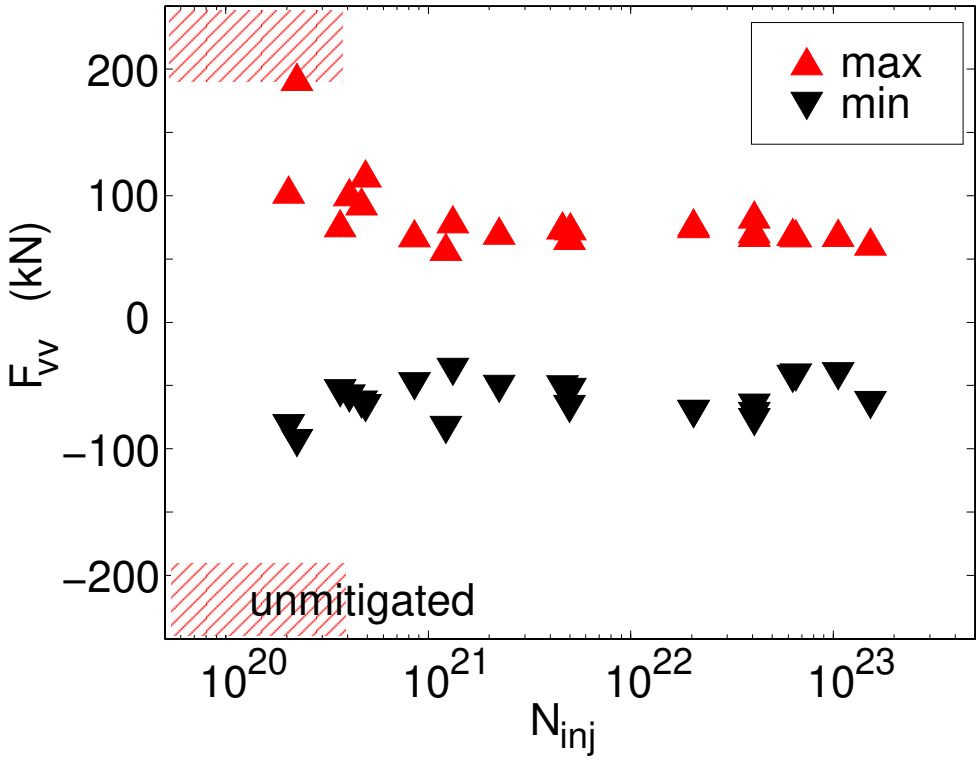

Figure 7: Maximum (max) and minimum (min) vertical force on the vacuum vessel (F_{vv}), measured by strain gauges, versus the number of injected neon atoms (N_{inj}).

[Show also figure w time traces]

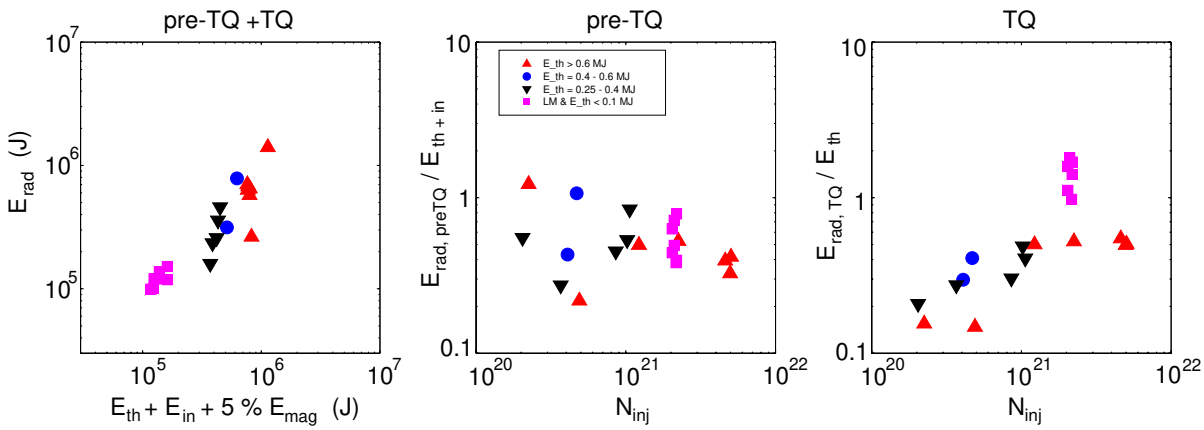

Figure 8: Left: energy radiated during the pre-TQ and TQ phases (E_{rad}) versus the energy available for dissipation, i.e. the sum of the target thermal energy (E_{th}), of the auxiliary energy in input (E_{in}) and 5 % of the magnetic energy (E_{mag}). Center: $E_{rad}/(E_{th} + E_{in})$ versus N_{inj} during pre-TQ. Right: E_{rad}/E_{th} versus N_{inj} during TQ.

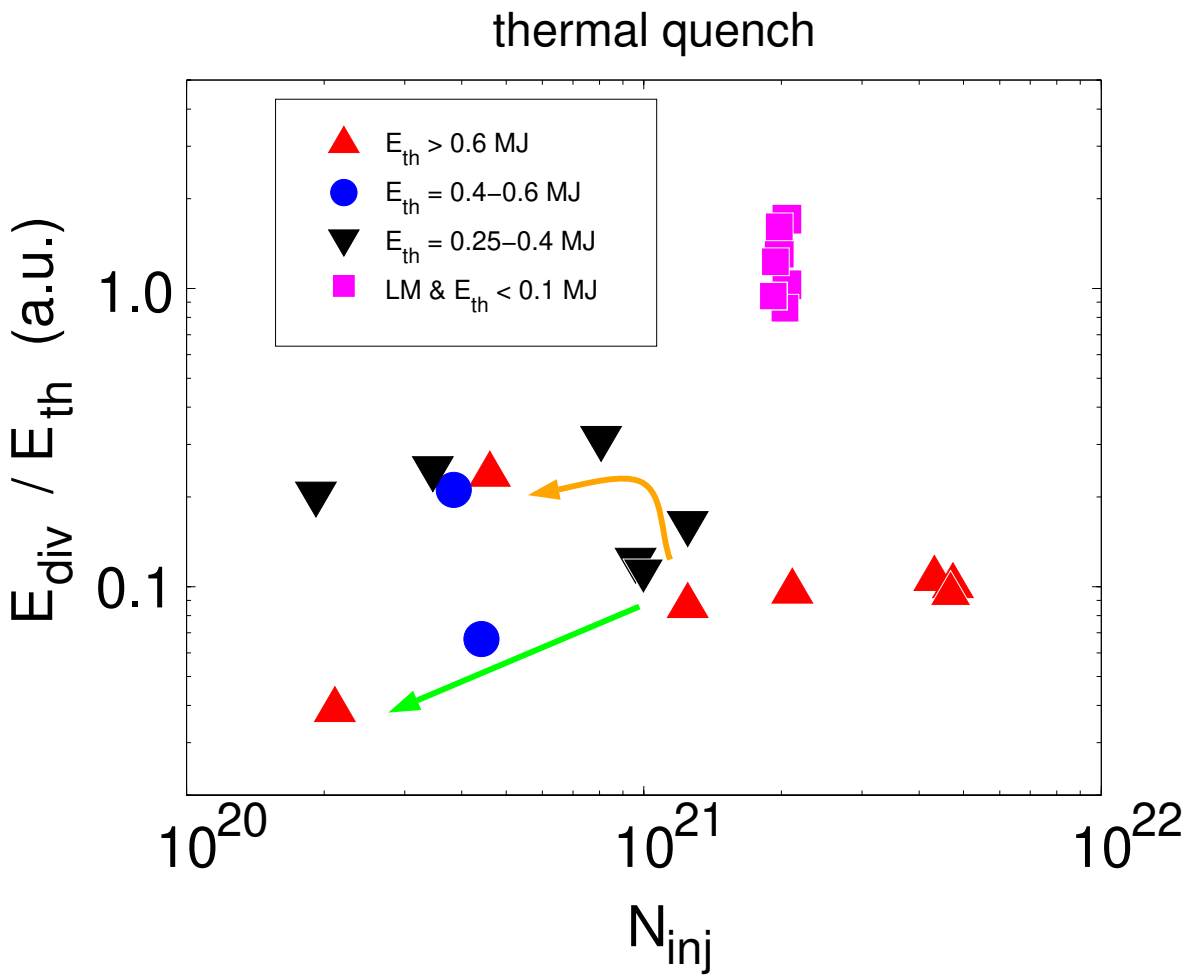

Figure 9: Energy deposited on a limited area of the outer divertor (E_{div}) during the thermal quench (TQ), normalized to the target thermal energy (E_{th}).

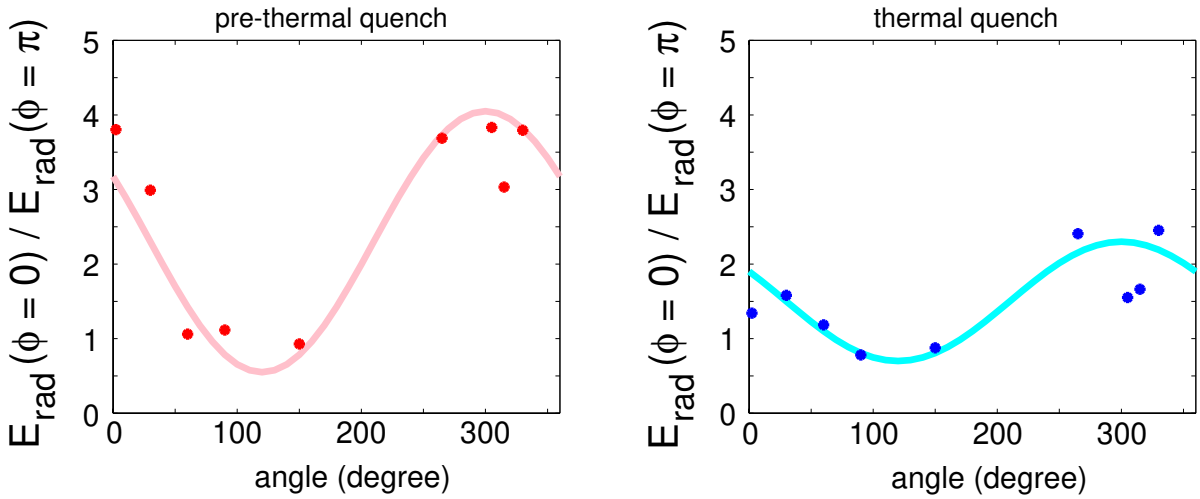

Figure 10: Ratio between the energy radiated in front of the gas injection location ($E_{rad}(\phi = 0)$) and the energy radiated in the sector 180 degree apart ($E_{rad}(\phi = \pi)$) during the pre- thermal quench (left) and thermal quench (right) versus position of the maximum n=1 component of the radial magnetic field, as measured by the saddle coils on the HFS.

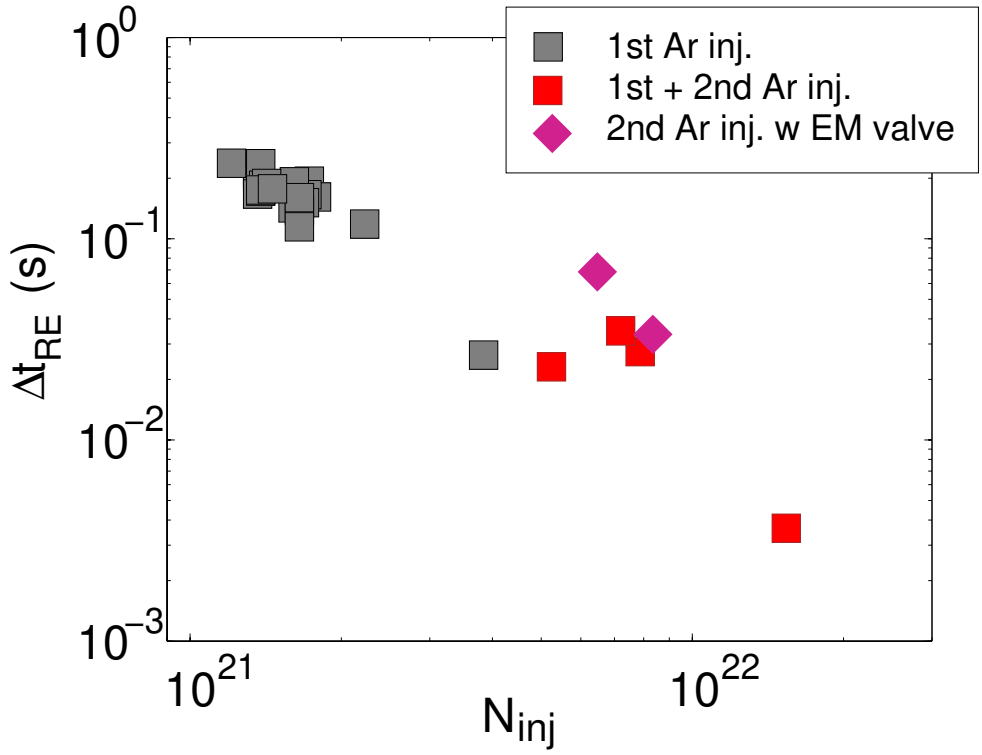

Figure 11: Life time of RE beam (Δt_{RE}) versus the total (i.e. $1^{st} + 2^{nd}$) injection, amount of argon injected (N_{inj}).

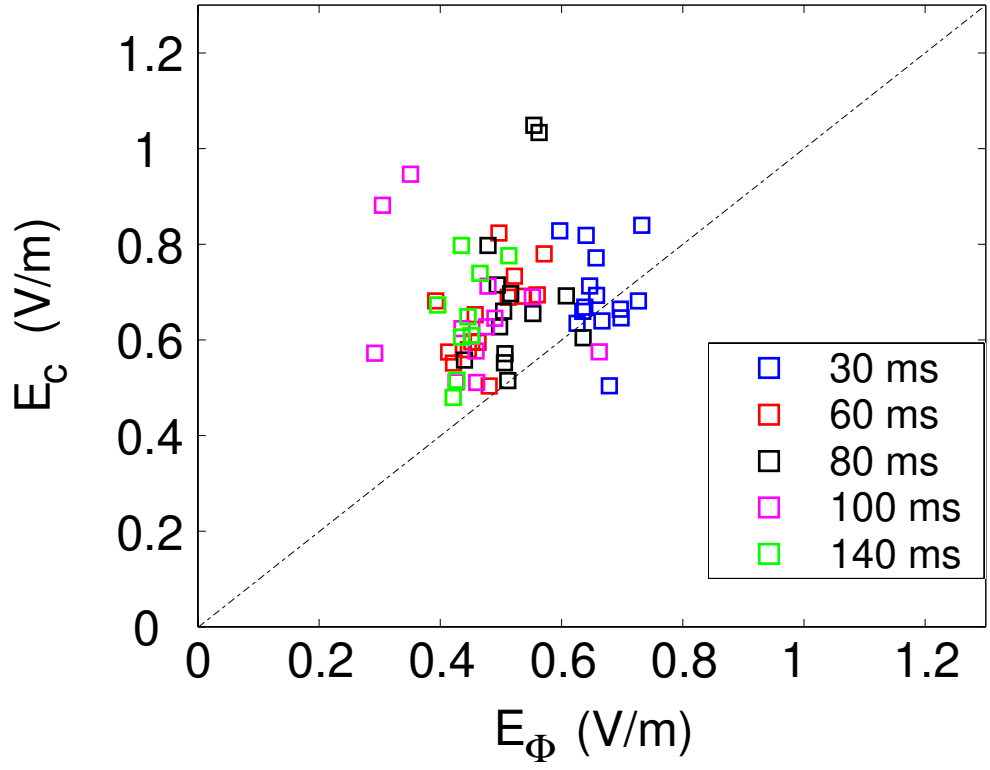

Figure 12: Critical electric field (E_c) versus the toroidal electric field (E_Φ) at different times during the RE beam.

[delete the early points of RE w 2-nd injection]